10

Axisymmetric Flows Driven by the Injection of Current

Matters of elegance should be left to the tailor and to the cobbler.

A. Einstein 1916

When an electric current is made to pass through a liquid-metal pool it causes the metal to pinch in on itself. That is to say, like-signed currents attract one another, and so each part of the pool is attracted to every other part. When the current is perfectly uniform, the only effect is to pressurise the liquid. However, often the current is non-uniform; for example, it may spread radially outwards from a small electrode placed at the surface of the pool. In such cases the radial pinch force will also be non-uniform, being largest at places where the current density is highest (near the electrode). The (irrotational) pressure force, $-\nabla p$, is then unable to balance the (rotational) Lorentz force. Motion results, with the fluid flowing inward in regions of high current density and returning through regions of small current.

Perhaps the first systematic experimental investigation of the 'pinch effect' in current-carrying melts was that of E F Northrup who, in 1907, injected current into pools of mercury held in a variety of different configurations. It should be noted, however, that industrial metallurgists have been routinely passing large currents through liquid metals since 1886, when Hall and Héroult first developed the aluminium reduction cell and von Siemens designed the first electric-arc furnace. One of the many descendants of the electric-arc furnace is vacuum-arc remelting (VAR).

10.1 The VAR Process and a Model Problem

10.1.1 The VAR process

There are occasions when an ingot cast by conventional means is of inadequate quality, either because of excessive porosity in the ingot or else because it contains unacceptably high levels of pollutants (oxides,

refractory material and so on). This is particularly the case in the casting of high-temperature melts, such as titanium or nickel-based alloys, which tend to react with (or erode) the refractory vessel in which they are melted. It also arises when the components fashioned from the ingot are expected to exhibit consistently high levels of strength and ductility. Here, aerospace applications come to mind. In such situations it is normal to improve the ingot quality by remelting it in a partial vacuum, burning off the impurities, and then slowly casting a new ingot. This is achieved by a process known as vacuum-arc remelting.

In effect, VAR resembles a giant version of electric welding (Figure 10.1). The initial ingot, which may be a metre in diameter and several metres long, is used as an electrode. A large current is passed down the ingot (electrode) and an arc is struck between the tip of the ingot and a cooled metal surface. The ingot then starts to melt, and droplets of molten metal fall through the plasma arc to form a pool on the cooled plate. As the electrode is slowly melted, so a new ingot forms beneath it. The entire process takes place in a partial vacuum. The metallurgical structure of the final ingot depends critically on the temperature distribution and fluid motion within the molten pool and this, in turn, depends on the gravitational and Lorentz forces acting on the melt. There is some incentive, therefore, to characterise the flow within the pool and to determine its dependence on such factors as ingot current.

In this regard a useful model problem is the following. Suppose we have a hemispherical pool of radius R. The boundaries of the pool are conducting, and a current, I, is introduced into the pool via an electrode

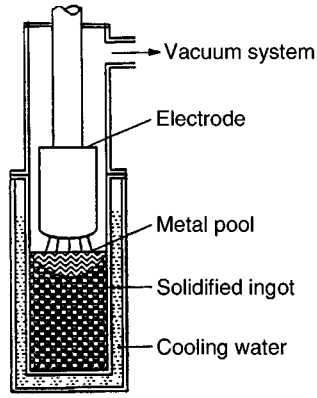

Figure 10.1 Vacuum-arc remelting.

of radius r_0, the current density being uniform in the electrode. We neglect buoyancy forces and try to determine the motion within the pool as a function of I, r_0 and R.

This model problem is relevant, not only to VAR, but also to electro-slag remelting of ingots and electric-arc welding. The flow pattern is as shown in Figure 10.2. Like-signed currents attract each other, and so the current passing through the pool causes the liquid to pinch in on itself. This radially inward force is greatest at the surface, where $|\mathbf{J}|$ is most intense, and weakest at the base of the pool where $|\mathbf{J}|$ is smallest. The net result is a flow which converges at the surface.

This seemingly simple problem has been the subject of a myriad of papers. Indeed, an entire book has been devoted to it (Bojarevics et al., 1989). Yet, arguably, we know less about this problem than about most of the other flows discussed in Part B of this book. One reason is that the apparently simple flow shown in Figure 10.2 turns out to be surprisingly complex. For example, it becomes unsteady (and eventually turbulent) at surprisingly low Reynolds numbers, around $\mathrm{Re} \sim 10$. It is also extremely sensitive to weak, stray magnetic fields, such as those associated with remote inductors or perhaps even the Earth's magnetic field. In particular, a stray magnetic field which is only 1% of the primary field (i.e. that field associated with the passage of the current through the pool) is enough to suppress completely the poloidal flow shown in Figure 10.2 and replace it by an intense swirling motion. It seems that, one way or another, the laminar flow shown in Figure 10.2 is somewhat ephemeral, evolving into something quite different at the slightest provocation. The word 'unstable' appears quite often in the literature.

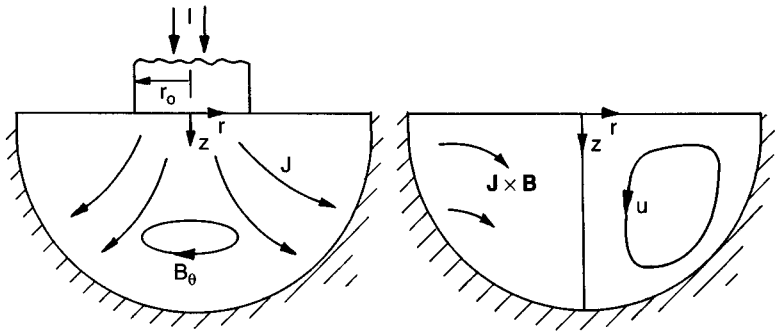

Figure 10.2 A model problem.

However, this is not the only reason that our attempts to understand this flow have been so unsuccessful. It turns out that the special case of a point electrode ($r_0 \to 0$) injecting current into a semi-infinite fluid ($R^{-1} = 0$) has an exact solution for laminar flow. Of course, exact solutions of the Navier–Stokes equations are extremely rare and beautiful things, and so it was natural for those first investigating this problem to focus on the semi-infinite-domain, point-electrode problem. In a sense this exercise has been successful: we now know a lot about this exact solution. Unfortunately, though, it turns out that the point-electrode problem tells us very little about the flow shown in Figure 10.2. That is to say, the special case $r_0 \to 0$, $R^{-1} = 0$ is a singular one, whose characteristics are often quite misleading in the context of real, confined flows. Yet a tradition grew up where a detailed, elegant analysis of some feature of the exact solution was performed, and then inferences were made about real, confined flows such as those observed in the laboratory. Unfortunately, when the experimental data were examined, the 'theory' was often found to be wanting. In short, we had been solving the wrong problem. (Perhaps we should have heeded Einstein's warning!)

There are a number of questions which naturally arise concerning the model problem shown in Figure 10.2.

(i) What is the direction and magnitude of the Lorentz force acting on the pool?
(ii) Why is there such a large difference in behaviour between real, confined flows and the point-electrode, semi-infinite-domain problem? Is there some fundamental physical difference between the two?
(iii) What does the exact solution of the (laminar) point-electrode problem tell us and can we transcribe *any* of its conclusions to real, confined flows?
(iv) Why do real, confined flows become unstable (and then turbulent) at such low Reynolds numbers?
(v) Given that any industrial flows will be turbulent, how does $\mathbf{u}$ scale with I, R and r_0 in a turbulent flow?
(vi) How does buoyancy influence this flow (the surface of the pool is assumed to be hotter than the sides)?
(vii) Why is the flow so sensitive to weak, stray magnetic fields, and does the laminar, point-electrode problem (about which we know so much) give us any hint as to the nature of this sensitivity?

(viii) Can we construct a quantitative theory which predicts the sensitivity of this flow to stray magnetic fields? Will this theory predict the unexpected emergence of swirl?

With the impatient reader in mind, these questions are listed in Table 10.1 along with some hints as to the answers. (Note that we use cylindrical polar coordinates (r, θ, z) throughout this chapter, and that the term 'azimuthal' refers to the θ components of a vector field, while 'poloidal' refers to the r–z components.)

Much of the discussion which follows (in Sections 2 to 7) is based on a variety of energy arguments. It seems appropriate to review first the key energy equations which are relevant to our model problem.

10.1.2 Integral constraints on the flow

The Lorentz force, $\mathbf{J} \times \mathbf{B}$, does work on the fluid. This causes the kinetic energy of the flow to rise until such time as the viscous dissipation matches the rate of working of $\mathbf{J} \times \mathbf{B}$. If, for a given current, we can characterise the relationship between $(\mathbf{J} \times \mathbf{B}) \cdot \mathbf{u}$ and the rate of dissipation of energy, then we should be able to estimate the magnitude of $|\mathbf{u}|$. Thus the key to estimating $|\mathbf{u}|$ lies in determining the mechanism by which the fluid dissipates the energy injected into the flow. For example, is the dissipation confined to boundary layers or are internal shear layers set up, and what happens to those streamlines which manage to avoid all such dissipative layers? There are two energy equations of importance here; both rest on the steady version of the Navier–Stokes equation:

$$0 = \mathbf{u} \times \boldsymbol{\omega} - \nabla\left(p/\rho + u^2/2\right) + \nu\nabla^2\mathbf{u} + \mathbf{F} \tag{10.1}$$

(Here $\mathbf{F}$ is the Lorentz force per unit mass.) The first equation comes from integrating (10.1) around a closed streamline, which yields

$$\oint \mathbf{F} \cdot d\mathbf{l} + \nu \oint \nabla^2\mathbf{u} \cdot d\mathbf{l} = 0 \tag{10.2}$$

This represents the balance between the work done by the Lorentz and viscous forces acting on a fluid particle as it passes once around a closed streamline. The second energy equation comes from taking the product of (10.1) with $\mathbf{u}$ and then integrating the result over the entire domain. Noting that terms of the form $\mathbf{u} \cdot \nabla(\sim) = \nabla \cdot (\sim \mathbf{u})$ integrate to zero and that $\left(\nabla^2\mathbf{u}\right) \cdot \mathbf{u} = \nabla \cdot (\mathbf{u} \times \boldsymbol{\omega}) - \boldsymbol{\omega}^2$, we find

$$\int \mathbf{F} \cdot \mathbf{u} dV = \nu \int \boldsymbol{\omega}^2 dV \tag{10.3}$$

Table 10.1. *Questions concerning the model problem shown in Figure 10.2*

	Question	Answer	Consult
(i)	What is the magnitude and direction of the Lorentz force?	Radial, of magnitude $-B_\theta^2/(\rho\mu r)$	10.2
(ii)	Why are confined and unconfined flows so different?	Two reasons. (a) Unconfined flows are free from intense, boundary-layer-dissipation. Confined flows are dominated by the balance between the work down by $\mathbf{J} \times \mathbf{B}$ and boundary-layer dissipation (b) The streamlines in unconfined flows do not close on themselves, so that we are free to 'impose' conditions in the far field	10.3.1
(iii)	Does the point-electrode, semi-infinite-domain problem tell us anything useful?	Yes, but only about the point-electrode, semi-infinite-domain problem	10.3.2
(iv)	Why do confined flows become unstable at such low values of Reynolds number?	We do not know, but it appears that the boundary layer becomes unstable at relatively low values of Re	10.3.3
(v)	How does $\mathbf{u}$ scale in a turbulent flow?	$\lvert\mathbf{u}\rvert \sim \dfrac{I(\mu/\rho)^{1/2}}{2\pi R}$	10.3.3
(vi)	What is the influence of buoyancy?	It tends to drive motion in the opposite direction	10.4
(vii)	Why is the flow so sensitive to weak, stray magnetic fields?	Stray fields produce an azimuthal torque which tends to induce swirl. It is much easier to spin a fluid in the azimuthal direction than generate the poloidal motion shown in Figure 10.2	10.5 10.7.1
(viii)	Does the point electrode problem help explain this sensitivity to stray fields?	Probably not	10.6
(ix)	Can we construct a quantitative theory which predicts the unexpected emergence of swirl?	Yes. This relies on establishing a balance between the centripetal acceleration and the poloidal Lorentz force	10.7.2, 10.7.3

This represents a global balance between the rate of working of the Lorentz force and the viscous dissipation. Either (10.2) or (10.3) may be used to estimate the magnitude of **u** provided, of course, that **F** is known. Actually, it is not difficult to show that (10.3) is equivalent to evaluating (10.2) for each streamline in the flow and then adding together all such integrals (see Example 1 at the end of the chapter).

In the remainder of this chapter we shall see how (10.2) and (10.3) may be used to determine the flow in our model problem. The discussion is arranged as follows. In Section 2 we determine the Lorentz force associated with the current. Next, in Section 3, we discuss the structure of, and scaling laws for, this flow. Here particular attention is given to the special (if somewhat misleading) case in which $r_0 \to 0$ and R recedes to infinity. As explained above, the reason for the extended discussion for this (singular) case is that, rather surprisingly, it possesses an exact, self-similar solution. Traditionally, a great deal of emphasis has been placed on this exact solution.

Next, in Section 4, we note that in both VAR and arc-welding the upper surface of the pool is hotter than its sides. We therefore consider the influence of buoyancy on the Lorentz-driven flow. Buoyancy forces tend to drive a flow which diverges at the surface of the pool; precisely opposite to the Lorentz-driven flow. Thus there is a direct competition between the buoyancy and Lorentz forces. We determine the conditions under which buoyancy prevails.

We conclude, in Sections 5 to 7, with a discussion of an old, but still controversial, subject. We shall examine the influence of weak, stray magnetic fields on the fluid motion. As mentioned above, these stray fields have a disproportionate influence on the pool dynamics, suppressing the poloidal flow and driving an intense swirling motion. There has been a great deal written about this problem. In Section 5 we review the experimental evidence for the extraordinary sensitivity of the confined, current-carrying fluids to a weak, stray magnetic field. Next, in Section 6, we discuss the traditional, if flawed, explanation of the phenomenon. We conclude, in Section 7, with a modern interpretation.

10.2 The Work Done by the Lorentz Force

If we are to use (10.2) or (10.3) to estimate the magnitude of **u** then the first step is to evaluate the Lorentz force, **F**. Let us assume that the entire geometry is axisymmetric. We shall use cylindrical polar coordinates (r,

θ, z) with the origin at the pool's surface, as shown in Figure 10.3. Evidently, the current is poloidal $(J_r, 0, J_z)$, and this gives rise to an azimuthal magnetic field, $(0, B_\theta, 0)$ (see Figure 10.2). The magnetic field and current density are related via Ampère's circuital law, according to which

$$2\pi r B_\theta = \mu \int_0^r (2\pi r J_z) dr \tag{10.4}$$

An expression for the corresponding Lorentz force per unit mass is given in Chapter 5, Section 6.1:

$$\mathbf{F} = \mathbf{J} \times \mathbf{B}/\rho = -\frac{B_\theta^2}{\rho \mu r} \hat{\mathbf{e}}_r \tag{10.5}$$

This drives a flow which converges at the surface, where B_θ is largest, and diverges near the base of the pool (Figure 10.2).

There are certain cases, such as electric-arc welding, where $r_0 \ll R$. Here we might try to model the electrode as a point source of current. In these situations it is useful to introduce the additional (spherical polar) coordinates, s and ϕ, defined by $s^2 = r^2 + z^2$ and $\cos\phi = r/s$. It is not difficult to show that, for a point source of current,

$$\mathbf{J} = \frac{I}{2\pi s^2}(\cos\phi, 0, \sin\phi), \qquad \mathbf{F} = -\frac{\mu I^2}{4\pi^2 \rho r^3}(1 - \sin\phi)^2 \hat{\mathbf{e}}_r \tag{10.6, 10.7}$$

Let us now return to the more general case of finite r_0. Given the importance of the integral constraint (10.2), it seems appropriate to evaluate the work done by **F**. The simplest case to consider is a fluid particle which follows a streamline lying close to the boundary. Integrating **F** along the surface from point 'a' ($r = R, z = 0$) in Figure 10.3 to point 'b' ($r = 0, z = 0$) gives

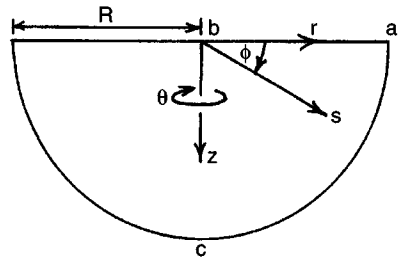

Figure 10.3 Coordinate system.

$$\int_a^b \mathbf{F} \cdot d\mathbf{l} = \frac{\mu I^2}{4\pi^2 \rho r_0^2}\left(1 - \frac{r_0^2}{2R^2}\right) \tag{10.8}$$

The integral of $\mathbf{F}$ along the symmetry axis is zero, since $B_\theta = 0$ on $r = 0$, while the integral along the curved boundary depends on the aspect ratio r_0/R. When $r_0 \ll R$, (10.7) yields

$$\int_c^a \mathbf{F} \cdot d\mathbf{l} = \frac{\mu I^2}{4\pi^2 \rho R^2}\left[\frac{1}{2} - \ln 2\right] \tag{10.9}$$

from which

$$\boxed{\oint \mathbf{F} \cdot d\mathbf{l} = \frac{\mu I^2}{4\pi^2 \rho r_0^2}\left[1 - \frac{r_0^2}{R^2}\ln 2\right]} \tag{10.10}$$

This represents the work done by $\mathbf{F}$ on a fluid particle as it completes one cycle in the r–z plane. It is the balance between this integral and the viscous dissipation which determines the magnitude of the induced velocity. It is interesting to note that $\oint \mathbf{F} \cdot d\mathbf{l}$ tends to infinity as $r_0 \to 0$. This, in turn, suggests that there is something singular about the point electrode problem. We shall return to this issue shortly.

10.3 Structure and Scaling of the Flow

10.3.1 Differences between confined and unconfined flows

Both electric welding and VAR are characterised by the facts that: (i) the electrode has a finite size; (ii) the Reynolds number is high and the flow turbulent; (iii) the presence of the boundary at $s = R$ controls the magnitude of $\mathbf{u}$ since most of the dissipation occurs in the boundary layers. Nevertheless, most studies of this problem have focused on laminar flow driven by a point electrode in a semi-infinite domain! The reason for this concentration on an idealised problem was the discovery by Shercliff (1970) and others that there exists an exact solution of the Navier–Stokes equation for the case of a point electrode on the surface of a semi-infinite domain. Unfortunately, as noted above, these point-electrode, semi-infinite-domain problems can be quite misleading in the context of real, confined flows. There are three key differences. First, the streamlines in the semi-infinite problem converge toward the axis but

do not close on themselves (Figure 10.4). They are therefore free from integral constraints of the form

$$\oint_C \mathbf{F} \cdot d\mathbf{l} + \nu \oint_C \nabla^2 \mathbf{u} \cdot d\mathbf{l} = 0 \tag{10.11}$$

where C is a closed streamline. Integrals such as (10.11) determine the magnitude of $\mathbf{u}$ in closed-streamline problems, yet are irrelevant in cases where the streamlines are open. Thus, for example, any difference between $\int \mathbf{F} \cdot d\mathbf{l}$ and $\nu \int \nabla^2 \mathbf{u} \cdot d\mathbf{l}$ in the semi-infinite problem simply appears as a difference in the energy of the incoming and outgoing fluid.

The second, related, difference lies in the fact that flows in confined domains are subject to (intense) dissipation associated with the boundary layer at $s = R$. This is significant since, as we have seen,

$$\int_V \mathbf{F} \cdot \mathbf{u} dV = \nu \int_V \omega^2 dV \tag{10.12}$$

That is to say, the global rate of working of $\mathbf{F}$ must be balanced by viscous dissipation. For confined domains the right-hand side of (10.12) is dominated by the boundary-layer dissipation and so we might expect the boundary layers to determine the magnitude of $\mathbf{u}$. However, there are no boundary layers in the infinite-domain problem, and so we might expect the characteristic velocity in confined and unconfined problems to be rather different.

The third difference is evident from (10.10). The point-electrode problem represents a singular (and somewhat artificial) problem in which the work done by $\mathbf{F}$ on the fluid becomes infinite:

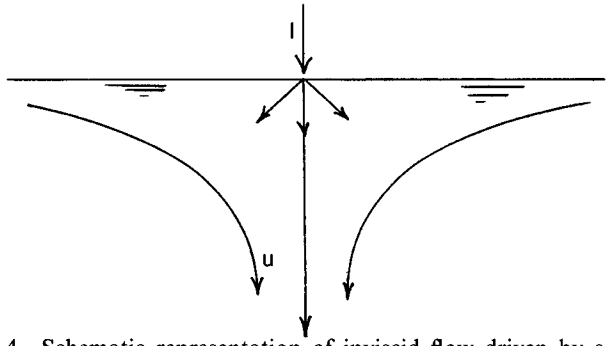

Figure 10.4 Schematic representation of inviscid flow driven by a point electrode.

$$\oint \mathbf{F} \cdot d\mathbf{l} = \frac{\mu I^2}{4\pi^2 \rho r_0^2} \to \infty$$

The implication is that, whenever ν is small, a fluid particle will acquire an infinite amount of kinetic energy as it passes by the electrode. This turns out to be the case, and it is the hallmark of these point-electrode, semi-infinite-domain problems that, as ν becomes small (Re becomes large), a singularity appears in the velocity field. Indeed, it is the combination of a self-similar solution (which makes the algebra clean) plus the intriguing appearance of a singularity in $\mathbf{u}$ which has made this point-electrode problem such a popular subject of study. It should be emphasised, however, that the appearance of a singularity in $\mathbf{u}$ is simply an artefact of the (unphysical) assumption that r_0 is vanishingly small.

All in all, it would seem that confined and unconfined flows represent quite different problems. Our primary concern here is in confined flows, such as those which occur in VAR or electric welding. Nevertheless, since the bulk of the literature addresses the semi-infinite-domain, point-electrode problem, it would seem prudent to review first the key features of such flows.

10.3.2 Shercliff's self-similar solution for unconfined flows

Let us consider a semi-infinite domain and look for a solution of (10.1) in which $\mathbf{F}$ is given by the point electrode distribution (10.7). It is convenient to introduce the Stokes streamfunction defined by

$$\mathbf{u} = \left(-\frac{1}{r}\frac{\partial \psi}{\partial z}, 0, \frac{1}{r}\frac{\partial \psi}{\partial r} \right) \tag{10.13}$$

and to take the curl of (10.1), converting it into a vorticity transport equation:

$$\mathbf{u} \cdot \nabla\left(\frac{\omega_\theta}{r}\right) = \frac{1}{r}\frac{\partial F}{\partial z} + \nu\left[\nabla^2\left(\frac{\omega_\theta}{r}\right) + \frac{2}{r}\frac{\partial}{\partial r}\left(\frac{\omega_\theta}{r}\right)\right] \tag{10.14}$$

We now look for self-similar solutions of (10.14) of the form

$$\psi = -sg(\eta), \qquad \eta = \sin\phi = z/s \tag{10.15}$$

Let us evaluate the various terms in (10.14). After a little algebra we find that

$$\mathbf{u}\cdot\nabla(\omega_\theta/r) = -(g^2)'''/(2s^5), \qquad \frac{1}{r}\frac{\partial F}{\partial z} = \frac{\mu I^2}{4\pi^2\rho s^5}\left[(1+\eta)^2\ln(1+\eta)\right]'''$$

$$\nabla^2\left(\frac{\omega_\theta}{r}\right) + \frac{2}{r}\frac{\partial}{\partial r}\left(\frac{\omega_\theta}{r}\right) = \frac{1}{s^5}\left[(1-\eta^2)g' + 2\eta g\right]''' \tag{10.16}$$

where the primes represent differentiation with respect to η. Substituting these into (10.14) and integrating three times we obtain the governing equation for g,

$$g^2 + 2K(1+\eta)^2\ln(1+\eta) + 2\nu[(1-\eta^2)g' + 2\eta g] = a\eta^2 + b\eta + c \tag{10.17}$$

Here

$$\boxed{K = \frac{\mu I^2}{4\pi^2\rho}} \tag{10.18}$$

and a, b and c are constants of integration. The simplest case to consider is the inviscid one. The constants a, b and c are then determined (in part) by the requirements that: (i) u_z is zero on $z = 0$; (ii) u_r is zero on $r = 0$. These conditions are equivalent to demanding that $g(0) = g(1) = 0$. Inspection of the inviscid equation yields $c = 0$, $a + b = 8K\ln 2$, from which

$$g^2 = K[a\eta(\eta-1) + (8\ln 2)\eta - 2(1+\eta)^2\ln(1+\eta)] \tag{10.19}$$

This represents a flow of the type shown in Figure 10.4

Of course, the question now is: what determines a? Before answering this question it is instructive to return to (10.8), which gives the integral of $\mathbf{F}$ along the surface from $r = R$ to $r = 0$. If we let R recede to infinity then we obtain

$$\int_{r=\infty}^{r=0} \mathbf{F}\cdot d\mathbf{l} = \frac{\mu I^2}{4\pi^2\rho r_0^2} = \frac{K}{r_0^2} \tag{10.20}$$

This represents the work done on a fluid particle as it moves along the surface under the influence of the Lorentz force. Recall that r_0 is the radius of the electrode. For a point source of current this integral diverges. Evidently, in the case of a point electrode, an infinite amount of work is done on each fluid particle as it moves radially inward along the surface. This suggests that something is going to go wrong with our inviscid solution, since we have no mechanism for dissipating the energy

created by **F**. In practice, this manifests itself in the following way. We could try to fix 'a' by demanding that u_r is finite on the surface (i.e. the incoming flow has finite energy). In such cases we find that u_z is infinite on the axis (i.e. the outgoing flow has infinite energy), which is an inevitable consequence of (10.20). The details are simple to check. The requirement that u_r is finite on $z = 0$ demands that, $a = 8 \ln 2 - 2$, from which

$$g^2 = K[(8 \ln 2 - 2)\eta^2 + 2\eta - 2(1 + \eta)^2 \ln(1 + \eta)] \tag{10.21}$$

Near the axis, however, this leads to an axial velocity of

$$u_z = -\frac{K^{1/2}(3 - 4 \ln 2)^{1/2}}{r}$$

Evidently, u_z diverges as r tends to zero.

If we now reinstate viscosity into our analysis, then it seems plausible that a regular solution of (10.18) will emerge, provided, of course, that the viscous stresses are large enough to combat the tendency for **F** to generate an infinite kinetic energy. In practice, this is exactly what occurs. When the (Reynolds-like) parameter $K^{1/2}/\nu$ is less than ~ 7, regular solutions of (10.18) exist without any singularity in **u**. For higher values of $K^{1/2}/\nu$, u_z becomes singular on the axis (Bojarevics et al., 1989). Of course, this does not imply that anything special, such as an instability, occurs at the critical value of $K^{1/2}/\nu$. It merely means that our attempt to find a self-similar solution of the form $\psi \sim sg(\eta)$ has failed. Notice that $K^{1/2}/\nu = 7$ corresponds to a relatively low current, of around 1 Amp, which is several orders of magnitude smaller than the currents used in industrial applications.

10.3.3 Confined flows

Let us now return to flows which are confined to the hemisphere $s < R$ and in which the electrode has a finite radius, r_0, of order R. In VAR and electric welding the Reynolds number is invariably high. It is natural, therefore, to ask two questions:

(i) what is the structure of the laminar flow when Re is large?
(ii) what is the magnitude of **u** when the flow becomes turbulent?

The answer to the first of these questions is surprising: it is likely that there are no stable, laminar flows at moderate-to-high values of Re! The reasons for this are discussed in detail in Kinnear & Davidson (1998) and

we will give here only a brief summary of the arguments. Suppose that we have a steady, laminar flow and that $r_0 \sim R$, then the key equation is (10.2)

$$\oint \mathbf{F} \cdot d\mathbf{l} + \nu \oint \nabla^2 \mathbf{u} \cdot d\mathbf{l} = 0 \tag{10.22}$$

This integral constraint is powerful. It must be satisfied by *every* closed streamline. When Re is of the order unity (or less) it tells us that $u \sim FR^2/\nu$, where F is a characteristic value of $|\mathbf{F}|$. Now suppose that Re is large so that boundary layers form on the wall $s = R$. Inside the boundary layer the viscous dissipation is intense, while outside it is small. The boundary thickness, δ, is determined by the force balance $(\mathbf{u} \cdot \nabla)\mathbf{u} \sim \nu \nabla^2 \mathbf{u}$, which gives $\delta \sim (Re)^{-1/2} R$. Thus our integral equation applied to a streamline lying close the boundary yields

$$FR \sim (\nu u R)/\delta^2 \sim u^2$$

For a streamline away from the boundary, however, $\nabla^2 \sim R^{-2}$, and so

$$FR \sim (\nu u R)/R^2 \sim \nu u / R$$

The implication is that the flow in the boundary layer scales as $u_b \sim (FR)^{1/2}$, while that in the core scales according to $u_c \sim FR^2/\nu$, which is much larger than u_b. However, this cannot be so, since the velocity scale in the boundary layer is set by the core velocity. Clearly, something has gone wrong!

The numerical experiments discussed in Kinnear & Davidson (1998) suggest that nature resolves this dilemma in an unexpected way. At surprisingly low Reynolds numbers, of the order of 10, the flow becomes unstable and starts to oscillate. The integral equation (10.22) is then irrelevant. The oscillation consists of a periodic 'bursting' motion in the boundary layer which gives rise to a continual exchange of fluid between the dissipative boundary layer and the less dissipative core. If we now increase Re a little further, the flow becomes turbulent, which brings us to our second question.

We wish to determine how $|\mathbf{u}|$ scales with I and R in a turbulent flow. Let us apply (10.22) to the time-averaged streamlines of a turbulent flow, with Reynolds stresses replacing the laminar shear stress. Noting that, for a streamline close to the boundary, (10.8) yields

$$\oint \mathbf{F} \cdot d\mathbf{l} \sim K/2R^2$$

(assuming $r_0 \sim R$), we obtain

$$\frac{K}{2R^2} \sim \frac{\pi R}{2} \frac{\tau_w}{\rho \delta_w} \tag{10.23a}$$

Here τ_w and δ_w are the wall shear stress and the characteristic length scale for gradients in τ near the wall. Now $\tau_w/\rho \sim (u')^2$ and so (10.23a) can be used to estimate the turbulence level in the pool:

$$\frac{K}{2R^2} \sim \frac{\pi R}{2} \frac{(u')^2}{\delta_w} \tag{10.23b}$$

We now take $u' \sim u/3.5$ and $\delta_w \sim R/10$, where u is a typical mean velocity. (These estimates are typical of a confined, turbulent flow, as observed in induction furnaces.) In this case (10.23b) yields

$$\boxed{u \sim 0.6 \frac{K^{1/2}}{R} \sim 0.6 \frac{(\mu/\rho)^{1/2} I}{2\pi R}} \tag{10.24}$$

Velocities compatible with (10.24) are indeed observed.

10.4 The Influence of Buoyancy

So far we have neglected the buoyancy forces acting on the pool. In VAR these can be significant. Indeed, in some cases, they are the dominant forces acting on the liquid. It is useful to start by considering two extremes: one in which buoyancy may be neglected by comparison with $\mathbf{J} \times \mathbf{B}$, and the other in which buoyancy greatly outweighs the Lorentz force. These two extremes are shown in Figure 10.5. Notice that the Lorentz and gravitational forces tend to drive motion in opposite directions.

In Chapter 9, Section 5 we discussed natural convection in an axisymmetric cavity driven by a difference in temperature, ΔT, between the surface and the boundary. We showed that the maximum velocity in the pool is of the order of

$$\hat{u} \sim \frac{\alpha}{R} \left(\frac{g\beta R^3 \Delta T}{\alpha^2} \right)^{3/7} = \frac{\alpha}{R} (Gr)^{3/7} \tag{10.25}$$

where α is the thermal diffusivity and β the expansion coefficient. Actually, it turns out that (Davidson & Flood, 1994),

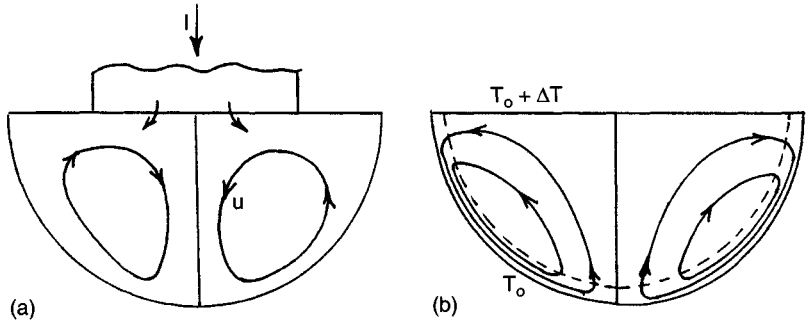

Figure 10.5 Two extremes in vacuum-arc remelting: (a) buoyancy forces are neglected; (b) the Lorentz forces are neglected.

$$\hat{u} = 1.3\frac{\alpha}{R}\left(\frac{g\beta R^3 \Delta T}{\alpha^2}\right)^{3/7} = 1.3\frac{\alpha}{R}(Gr)^{3/7} \tag{10.26}$$

Compare this with the other extreme where buoyancy is neglected and the flow is driven by $\mathbf{J} \times \mathbf{B}$:

$$\hat{u} \sim 0.6\frac{(\mu/\rho)^{1/2} I}{2\pi R} = 0.6\frac{K^{1/2}}{R} \tag{10.27}$$

In the case where the gravitational forces are dominant the fluid diverges at the surface and falls at the outer boundary. When the Lorentz forces dominate we have the opposite pattern, with the fluid converging at the surface. We might estimate the point of transition between these two flows by equating (10.26) and (10.27):

$$(Gr)^{3/7} \sim \frac{K^{1/2}}{\alpha} \tag{10.28}$$

Thus, the transition from buoyancy to Lorentz-driven flow should occur when the dimensionless parameter

$$\chi = K^{1/2}(Gr)^{-3/7}/\alpha \tag{10.29}$$

exceeds a number of order unity. In practice, it is found that the motion resembles a classical buoyancy-driven flow (of the type discussed in Chapter 9, Section 5.1) when χ is less than ~ 0.4. In such cases the Lorentz forces may be neglected when calculating $\mathbf{u}$. Conversely, when χ exceeds ~ 1.4 the buoyancy forces are unimportant. For intermediate values, $0.4 < \chi < 1.4$, the flow may have a complex, multi-cellular structure. This is illustrated in Figure I.6(b) (see introduction to Part B), where

the three figures correspond to $\chi = 0.5,\ 1.2,\ 1.5$. Apparently, modest changes in current can transform the motion from a buoyancy-dominated flow to a Lorentz force-dominated one. This change in flow regime is accompanied by a dramatic change in temperature distribution and of ingot structure. Interestingly, many commercial VAR units operate at just the verge of this transition.

10.5 Stability of the Flow and the Apparent Growth of Swirl

There are several industrial processes where current is injected into a liquid-metal pool, via its surface, but where the pool is also subject to a weak, stray magnetic field, perhaps associated with remote inductors. In such cases, the weak, stray magnetic field can have an astonishing influence on the motion in the pool, often to the detriment of the process. There is some incentive, therefore, to understand why stray magnetic fields have such a disproportionate influence on the pool motion. It is this question which occupies the remainder of this chapter.

10.5.1 An extraordinary experiment

Bojarevics et al. (1989) reported an intriguing experiment which exhibits a curious phenomenon, often called 'spontaneous swirl'. In this experiment, current is passed radially downward through an axisymmetric pool of liquid metal, as indicated in Figure 10.6. As we have seen, the interaction of the current density, $\mathbf{J}$, with its associated magnetic field, B_θ gives rise to a Lorentz force, $\mathbf{F} = \mathbf{J} \times \mathbf{B}/\rho$, which is poloidal. Of course, the resulting motion is also poloidal; at least this is the case at low levels

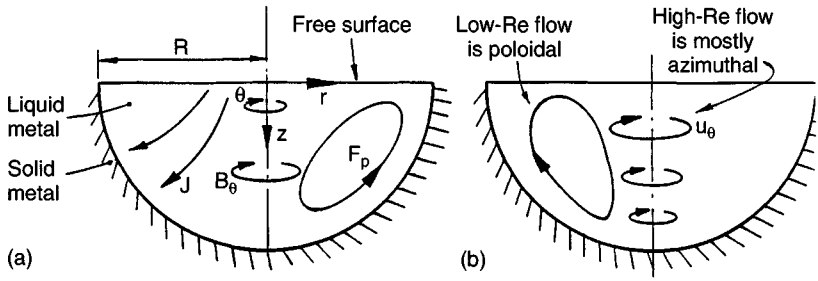

Figure 10.6 Experiment of Bojarevics et al. (a) Current flows down through the pool producing a poloidal force $\mathbf{F}_p = \mathbf{J}_p \times \mathbf{B}_\theta$. (b) At low levels of current the flow is poloidal, while a higher level of current initiates an intense swirling motion.

of forcing. At higher levels of current, though, something rather surprising occurs. The pool is seen to rotate, and this rotation is much more vigorous than the poloidal motion.

The observed rotation must, in some sense, result from a lack of symmetry in **J** or **B**. That is, a finite azimuthal force, F_θ, is required to maintain the swirl and in particular to overcome the frictional torque exerted on the pool by the boundaries. This additional force is thought to arise from the interaction of **J** with a weak, stray magnetic field. (For example, a vertical field B_z gives rise to an azimuthal force $-J_r B_z/\rho$.) Nevertheless, it is surprising that a force composed of a large poloidal component plus a weaker azimuthal contribution can give rise to a flow dominated by swirl, i.e. $u_\theta \gg u_r, u_z$. In the experiment the stray field arises in part from the Earth's magnetic field (Bojarevics et al., 1989). At the lower levels of current used (~ 15 Amps) the average magnetic field induced by the current on the pool surface is ~ 0.6 Gauss, which is comparable with the Earth's magnetic field. However, at the highest current levels (~ 1200 Amps) the average surface value of B_θ is around 42 Gauss, which is a factor of ~ 100 greater than the Earth's magnetic field. The key question, therefore, is why do low levels of azimuthal forcing give rise to disproportionately high levels of swirl?

Precisely the same phenomenon is seen at a larger scale in industrial processes such as vacuum-arc remelting of ingots. Here the stray magnetic field arises from inductors which carry current to and from the apparatus. Unless great effort is made to minimize the stray magnetic fields, an intense swirling motion is generated which can adversely affect the final product.

In all of these processes the Reynolds number, Re, is high, perhaps $300 \rightarrow 10^4$ in Bojarevic's experiment, and around 10^5 in industrial applications. It is almost certain, therefore, that these flows are turbulent. Moreover, the phenomenon seems to be particular to high Reynolds numbers, in the sense that there is a value of Re below which disproportionately high levels of swirl are not observed (Bojarevics et al., 1989). There is, however, a second threshold. That is, as we shall see, u_θ dominates the poloidal motion, $\mathbf{u}_p$, only when F_θ exceeds $\sim 0.01|\mathbf{F}_p|$. (We use subscript p to indicate poloidal components of **u** or **F**.) Below this threshold, the poloidal motion remains dominant, no matter what the value of Re. In particular, if $F_\theta \rightarrow 0$ then there is no swirling motion at all.

Let us summarise the experimental evidence. The term 'spontaneous swirl' is commonly used to describe high-Re flows in which the forcing

has both azimuthal and poloidal components, $\mathbf{F} = \mathbf{F}_\theta + \mathbf{F}_p$, but where the swirl dominates the motion despite the relative weakness of $\mathbf{F}_\theta$. That is,

$$u_\theta \gg |\mathbf{u}_p|, \qquad F_\theta \ll |\mathbf{F}_p|, \qquad (\mathrm{Re} \gg 1) \tag{10.30}$$

Note that it is not the appearance of abnormally high values of u_θ which typifies the experiment. Rather, it is the high value of the ratio $u_\theta/|\mathbf{u}_p|$ which is unexpected. This distinction may seem trivial, but it turns out to be important. Traditionally, this phenomenon was regarded as an instability, with the sudden appearance of swirl marking some instability threshold, rather like the sudden eruption of Taylor vortices in unstable Couette flow. Recently, however, it has been shown that this view is incorrect. We shall see that the magnitude of u_θ is simply governed by the (prescribed) magnitude of F_θ, and that there is nothing mysterious about the level of swirl. In fact, it is an unexpected suppression of $|\mathbf{u}_p|$ rather than a growth in u_θ, which typifies the observations.

10.5.2 There is no spontaneous growth of swirl!

We shall see that flows characterised by (10.30) do indeed exist, but that the phrase 'spontaneous swirl' is somewhat of a misnomer. Such flows would be better characterized by the term *poloidal suppression*. That is, the mystery is not that u_θ is unexpectedly large, but that, in the presence of swirl, $|\mathbf{u}_p|$ is disproportionately small. In fact, the magnitude of u_θ can always be estimated from the global torque balance,

$$\rho \int r F_\theta dV = \oint 2\pi r^2 \tau_\theta dl \tag{10.31}$$

Here l is a curvilinear coordinate measured along the pool boundary and τ_θ is the azimuthal surface shear stress. In a turbulent flow $\tau_\theta = c_f\left(\frac{1}{2}\rho u_\theta^2\right)$, where the skin friction coefficient c_f is, perhaps, of the order 10^{-2} (Davidson, Short and Kinnear, 1995). If R is a typical pool radius, this yields the estimate

$$u_\theta \sim \left(RF_\theta/c_f\right)^{1/2} \sim 10(RF_\theta)^{1/2} \tag{10.32}$$

Similar estimates may be made for laminar flow, but the details are unimportant. The key point is that u_θ is fixed in magnitude by F_θ.

We shall see that flows of type (10.30) arise from the action of the centrifugal force. That is, there are two driving forces for poloidal motion, the poloidal Lorentz force, $\mathbf{F}_p$, and the centrifugal force $-\left(u_\theta^2/r\right)\hat{\mathbf{e}}_r$, and it turns out that these conspire to eliminate each other.

Specifically, provided $\mathrm{Re} \gg 1$ and $F_\theta/|\mathbf{F}_p| >\sim 0.01$, the angular momentum of the fluid always distributes itself in such a way that these two forces almost exactly cancel (to within the gradient of a scalar), and that consequently, the poloidal motion is extremely weak. It is this balance between $\mathbf{F}_p$ and u_θ^2/r which underpins the experimental observations.

10.6 Flaws in the Traditional Explanation for the Emergence of Swirl

Traditionally, great significance has been attached to the fact that there appears to be a threshold value of Re above which swirl is dominant. This has led some researchers to conclude that the underlying poloidal motion is unstable and that the appearance of swirl is simply a manifestation of this instability. Consequently, it has been popular to study the breakdown of the self-similar poloidal flow associated with the injection of current from a point source located on the surface of a semi-infinite domain. As we have seen, these flows are characterised by the fact that the self-similar solution breaks down at a low value of Re. However, it turns out that a self-similar solution may be re-established above the critical value of Re if (somehow) just the right amount of angular momentum is injected into the flow at infinity. One of the deductions of this type of analysis is that flows which converge at the surface are potentially unstable, whereas those which diverge are stable. (Self-similar diverging flows may be realized using a slightly more complex, but still singular, arrangement of current injection.)

Perhaps the most thorough study of this type is that of Shtern & Barrero (1995). Like many before, they examined the breakdown of the self-similar flow, attributed this breakdown to an instability, and then suggested that these stability characteristics extend to confined domains, thus explaining the experimental observations. However, such a model problem differs from confined flows in two crucial respects. First, there is no outer frictional boundary and so this model problem is free from the integral constraint (10.31). That is, no external torque is required to maintain the swirl. Second, the streamlines in the self-similar solution do not close, but rather converge radially, as shown in Figure 10.7.

Now it happens that at $\mathrm{Re} \sim 7$ the similarity solution breaks down in the sense that the velocity on the axis becomes infinite (see Section 8.3.2). However, if just the right amount of swirl is introduced into the far field then, due to the radially inward convection of angular momentum, the singularity on the axis is alleviated. Thus, in semi-infinite domains there

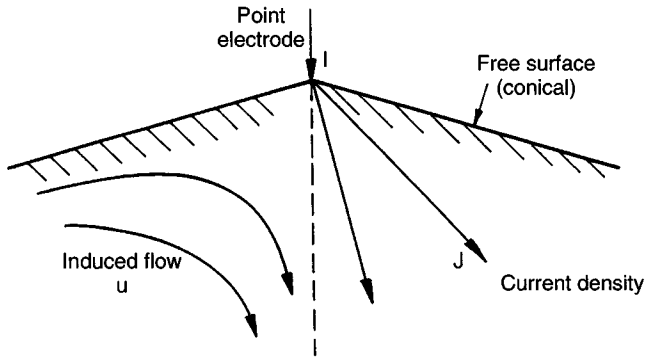

Figure 10.7 Geometry analysed by Shtern & Barrero.

exists the possibility of a bifurcation from a non-swirling to a swirling flow, provided, of course, that (somehow) nature provides just the right amount of angular momentum in the far field. This, according to traditional argument, is the origin of the experimental observations.

However, there are several fundamental objections to making the jump from infinite to confined flows. The first point to note is that the appearance of a singularity in the self-similar solution is simply an artefact of the (idealised) assumption of a point source of current (see (10.20)). Second, flow in a hemisphere bears little resemblance to the self-similar flow in an infinite domain. If R is the pool radius and r_0 the electrode radius, then a self-similar solution may be justified only in the small region $r_0 \ll \left(r^2 + z^2\right)^{1/2} \ll R$. In the experiments of Bojarevics et al. no such region exists ($R/r_0 \sim 45$). Third, the evidence for spontaneous swirl (poloidal suppression) is not restricted to point sources of current, but rather exists for many different distributions of current within the pool. An explanation of this behaviour which rests on the breakdown of a very particular class of motion (the self-similar flow) cannot explain the widespread occurrence of this phenomenon. Fourth, the infinite domain model relies on angular momentum being injected into the fluid in the far field. In confined domains, where does this angular momentum come from? If swirl exists in confined flows it must be maintained by an external torque, and the magnitude of this torque fixes the magnitude of the swirl. There can be no sudden 'eruption' of swirl due to an increase in Re. Fifth, according to the semi-infinite domain, point-electrode model, the sudden appearance of swirl occurs only if the flow converges at the surface. In practice, however,

this is not the case. As we shall see, the dominance of swirl ($u_\theta \gg |\mathbf{u}_p|$) occurs just as readily if the flow diverges at the surface. Clearly, we must seek an alternative explanation of the phenomenon.

10.7 The Rôle of Ekman Pumping in Establishing the Dominance of Swirl

10.7.1 A glimpse at the mechanisms

As a prelude to our detailed analysis we provide here a qualitative explanation of the phenomenon. The key point is this: it turns out to be easier to generate swirl in a hemispherical pool than poloidal motion. Suppose, for example, that we apply a force F_θ and measure the resulting swirl. We then remove F_θ and apply a force $\mathbf{F}_p$, again measuring the resulting motion. Then we would find that $u_\theta/F_\theta \gg |\mathbf{u}_p|/|\mathbf{F}_p|$. Thus small azimuthal forces, which result from the stray magnetic field, can give rise to a relatively large swirling motion. However, this is not the end of the story. This swirl, when large enough, arranges itself such that the centripetal acceleration, u_θ^2/r, counterbalances the poloidal Lorentz force (to within the gradient of a scalar). The poloidal flow then virtually disappears.

When we work through the details, it turns out that *Ekman pumping*, which played such an important rôle in Chapter 8, once again rears its head. You will recall that Ekman pumping is an inevitable by-product of confined swirl. Perhaps it is worth digressing for a moment to describe its main features. It is most simply understood in those cases where the Lorentz force is purely azimuthal ($\mathbf{F}_p = 0$), and so we now consider this special case.

Suppose that $\mathbf{F} = (0, F_\theta, 0)$ and the dominant motion is u_θ. Ekman pumping takes the form of a wall jet, as shown on the right of Figure 10.8. That is to say, the swirl induces a secondary poloidal motion consisting of a high-speed wall jet (Ekman jet) which runs downward within the boundary layer (the Ekman layer) and recirculates back up through the (almost) inviscid core flow. The driving force for the wall jet is a radial pressure gradient which is established in the core of the flow in order to maintain the centripetal acceleration of the swirling fluid. (This radial pressure gradient is unbalanced in the boundary layer where u_θ^2/r falls to zero.) It is important to note that Ekman pumping is not an incidental feature of this flow, but rather controls the magnitude of the swirl (see Chapter 8, Section 3). That is, in the steady state, the rate of generation of

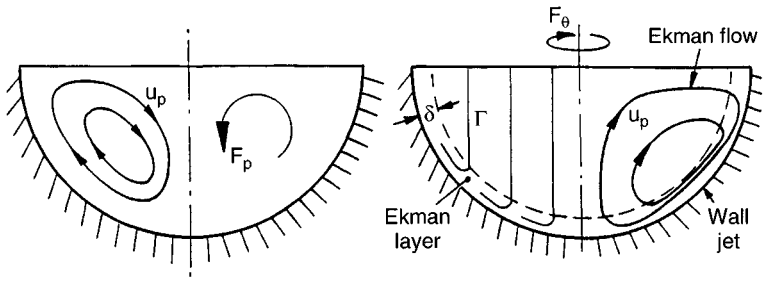

Figure 10.8 Flows driven by poloidal and azimuthal Lorentz forces. (a) Poloidal flow driven by a poloidal force. (b) Angular momentum contours and secondary Ekman flow induced by azimuthal force.

angular momentum and energy by F_θ must be matched by frictional dissipation, and it is this balance between the generation and dissipation of energy which dictates the steady state value of u_θ. However, the dissipation of energy is controlled by the Ekman pumping. It ensures that *all* the fluid particles are periodically flushed through thin, dissipative boundary layers, and this is the mechanism by which (10.2) is satisfied and a steady state is achieved.

We now return to the case in hand, where the dominant Lorentz force is poloidal rather than azimuthal. Suppose we have a pool of liquid metal into which we inject current (Figure 10.6). The current may be injected through a small region near the axis, or else distributed across the top of the pool. It does not matter. The current density in the metal is poloidal and induces an azimuthal magnetic field, $\mathbf{B}_\theta$. Suppose that, in addition, we have a weak, stray magnetic field, B_z. Then $\mathbf{F}$ comprises a strong poloidal component, $\mathbf{J} \times \mathbf{B}_\theta/\rho$, plus a weaker azimuthal contribution $\mathbf{J} \times \mathbf{B}_z/\rho$. Now suppose that, at least initially, B_z is so small that the induced swirl is much weaker than the primary poloidal motion. The distribution of $\mathbf{u}_p$ is then uniquely determined by the poloidal force (u_θ^2/r is negligible). Now consider the swirl. The governing equation for the angular momentum, $\Gamma = ru_\theta$, is

$$\frac{D\Gamma}{Dt} = \frac{\partial \Gamma}{\partial t} + \mathbf{u}_p \cdot \nabla \Gamma = rF_\theta + \nu_t \nabla \cdot \left[r^2 \nabla \left(\Gamma/r^2\right)\right] \tag{10.33}$$

Here the subscript on ν_t indicates that we have in mind a turbulent flow which we model rather crudely using a turbulent eddy viscosity. Let the pool be a hemisphere of radius R (the precise shape is not too important), and define an effective Reynolds number by $\mathrm{Re}_t = |\mathbf{u}_p|_{\max} R/\nu_t$. When Re_t

is large (typically it has a value of ~ 100), the shear stresses are dominant only in the boundary layers. Outside these regions (10.33) simplifies to

$$\frac{D\Gamma}{Dt} \approx rF_\theta + 0\left(Re_t^{-1}\right) \tag{10.34}$$

Evidently, angular momentum is generated in each fluid particle as a result of the azimuthal force and, provided boundary layers are avoided, this growth in Γ is constrained only by the relatively weak shear stresses in the core. Consequently, large values of swirl can build up, even though F_θ is small. From (10.33) we can estimate u_θ by equating the two terms on the right:

$$u_\theta/u_p \sim \left(F_\theta R/u_p^2\right) Re_t \tag{10.35}$$

Now suppose that we increase F_θ with $\mathbf{F}_p$ fixed, up to the point where u_θ and $\mathbf{u}_p$ are of similar magnitudes. (In practice we could do this by increasing the stray field B_z.) We have seen that, for small u_θ, $\mathbf{u}_p$ scales roughly as $|\mathbf{u}_p| \sim \left(|\mathbf{F}_p|R\right)^{1/2}$ (see equation (10.24), and so $u_\theta \sim \mathbf{u}_p$ when $F_\theta \sim Re_t^{-1}|\mathbf{F}_p| \sim 0.01|\mathbf{F}_p|$. Thus a small but finite azimuthal force can give rise to a significant (i.e. large) swirling motion. Once u_θ reaches a value of $\sim \mathbf{u}_p$, Γ ceases to play a passive rôle. It can react back on the poloidal motion through the centrifugal force $\left(-u_\theta^2/r\right)\hat{\mathbf{e}}_r$. There now exists an intriguing possibility. Suppose that Γ is distributed in such a way that $\left(-u_\theta^2/r\right)\hat{\mathbf{e}}_r$ balances $\mathbf{F}_p$ to within the gradient of a scalar:

$$\left(-u_\theta^2/r\right)\hat{\mathbf{e}}_r = \mathbf{F}_p + \nabla\phi + 0\left(Re_t^{-1}\right) \tag{10.36}$$

The driving force for poloidal motion then disappears (ϕ is absorbed into the pressure) and we are left with a swirling motion plus its associated (weak) Ekman pumping. If this were to occur, then the energy of the poloidal flow, and hence of the flow as a whole, should collapse as F_θ approaches a value of $\sim 0.01|\mathbf{F}_p|$. We shall see that this is precisely what happens, the resulting core flow being governed by

$$\mathbf{u}_p \cdot \nabla\Gamma = rF_\theta + 0(\nu_t), \qquad -\frac{\partial}{\partial z}\left(\frac{\Gamma^2}{r^3}\right) = \left(\nabla \times \mathbf{F}_p\right)_\theta + 0(\nu_t) \tag{10.37, 10.38}$$

Note that when the poloidal force is effectively eliminated, the poloidal motion reduces to a weak Ekman pumping. This not only dramatically reduces the energy of the poloidal flow, but also helps keep u_θ at a modest level. That is, if the only poloidal motion is Ekman pumping, all of the streamlines will be flushed through the dissipative Ekman layers where the angular momentum created by F_θ can be efficiently destroyed.

Evidently, if we can find core solutions for $\mathbf{u}_p$ and Γ which satisfy (10.37) and (10.38), then this represents an energetically favourable state. We shall see that these core equations are readily satisfied, and that the flow does indeed adopt this low-energy state. The net result is that when F_θ exceeds the modest threshold of $\sim 0.01|\mathbf{F}_p|$, the flow is dominated by swirl, despite the weakness of the azimuthal force.

10.7.2 A formal analysis

Let us assume that the flow is axisymmetric and the liquid pool occupies a hemisphere of radius R, as shown in Figure 10.6. The current enters the pool at the free surface and spreads radially outward as it passes down through the pool. In addition to the azimuthal field, we shall allow for a weak external magnetic field. For simplicity, we take this to be uniform and vertical. It is convenient to introduce the scaled magnetic field $\mathbf{C} = \mathbf{B}/(\rho\mu)^{1/2}$, which has the dimensions of velocity. Then, from (10.5), the Lorentz force (per unit mass) has components

$$\mathbf{F}_p = -\frac{C_\theta^2}{r}\hat{\mathbf{e}}_r, \qquad F_\theta = C_z\frac{\partial C_\theta}{\partial z} \tag{10.39, 10.40}$$

We shall take the flow to be turbulent and model the Reynolds stresses using a turbulent eddy viscosity, ν_t. The poloidal velocity field, $\mathbf{u}_p$, is uniquely determined by its vorticity, ω_θ. From (10.39), (10.40) and the Navier–Stokes equation, it is easy to show that the governing equations for ω_θ and Γ are

$$\mathbf{u}\cdot\nabla\Gamma = \frac{\partial}{\partial z}[rC_zC_\theta] + \nu_t\nabla\cdot\left[r^2\nabla(\Gamma/r^2)\right] \tag{10.41}$$

$$\mathbf{u}\cdot\nabla(\omega_\theta/r) = \frac{\partial}{\partial z}\left[\frac{\Gamma^2}{r^4} - \frac{C_\theta^2}{r^2}\right] + \nu_t\nabla\cdot\left[r^{-2}\nabla(r\omega_\theta)\right] \tag{10.42}$$

In terms of velocity, equation (10.42) may be uncurled to give the poloidal equation of motion

$$\mathbf{u}_p\cdot\nabla\mathbf{u}_p = -\nabla(p/\rho) + \left[\left(u_\theta^2 - C_\theta^2\right)/r\right]\hat{\mathbf{e}}_r + \nu_t\nabla^2\mathbf{u}_p \tag{10.43}$$

Evidently, whenever $u_\theta^2 - C_\theta^2$ is independent of z, the poloidal motion vanishes. Let us now look for solutions to these equations for the case where $F_\theta \ll |\mathbf{F}_p|$. We start by examining the energy balance in these confined flows. For a steady-on-average turbulent flow, (10.2) becomes

$$\oint \mathbf{F} \cdot d\mathbf{l} + \nu_t \oint \nabla^2 \mathbf{u} \cdot d\mathbf{l} = 0 \tag{10.44}$$

This integral constraint must be satisfied by every streamline in the time-averaged flow. This could be achieved by high levels of internal dissipation. However, when ν_t is small, it is natural to look for solutions in which the dissipation is largely confined to the boundary layers. This, in turn, requires that each streamline passes through a boundary layer. (Every streamline must satisfy (10.44).) If Ekman pumping is to supply the necessary entrainment mechanism, then it is essential that it dominates the poloidal flow, despite the weakness of F_θ. However, inspection of (10.41) and (10.42) shows that such a flow is indeed possible. Let Γ_c be the angular momentum distribution in the core of the flow, and $\Gamma_{cs}(r)$ be the corresponding value of Γ_c just outside the Ekman layer (at the same radius). Now suppose we require Γ_c to satisfy

$$\Gamma_c^2 = r^2 C_\theta^2 + f(r) \tag{10.45}$$

where $f(r)$ is an arbitrary function of radius. Then from (10.42) there is no source of poloidal motion other than Ekman pumping. This guarantees entrainment of all of the streamlines and so provides an effective dissipation mechanism for the flow. We now explore the consequences of this distribution of swirl. We shall see that there is no contradiction between (10.45) and the azimuthal equation of motion.

If (10.45) is satisfied, then the poloidal equations of motion (10.42) and (10.43) tell us nothing more about the core flow, other than the fact that Ekman pumping will occur. It remains to be seen if our assumed distribution of Γ, (10.45), is consistent with the azimuthal equation of motion (10.41). Now suppose that $C_z = -C_0$ where $C_0 > 0$. Since B_θ is a decreasing function of z this ensures that $\Gamma > 0$. Equation (10.41) now becomes, in the core of the flow,

$$\mathbf{u} \cdot \nabla \Gamma_c = -rC_0 \frac{\partial C_\theta}{\partial z} = rC_0 \left| \frac{\partial C_\theta}{\partial z} \right| \tag{10.46}$$

Clearly, as each fluid particle spirals upward through the core its angular momentum increases. We now ask if this is consistent with our assumed distribution of Γ: that is, is $\partial \Gamma_c / \partial z < 0$ compatible with (10.45)? The answer is 'yes'. Note that (10.45) gives

$$\Gamma_c \frac{\partial \Gamma_c}{\partial z} = r^2 C_\theta \frac{\partial C_\theta}{\partial z} < 0 \qquad (\text{since } \mathrm{J_r} > 0) \tag{10.47}$$

which is exactly what is required.

Finally, we must check that (10.45) is consistent with the azimuthal equation of motion in the Ekman layer. To this end we use (10.31), the integrated version of this equation:

$$\int rF_\theta dV = \pi \oint c_f \Gamma_{cs}^2 dl \tag{10.48}$$

Typically, c_f is of the order of 10^{-2} in a confined turbulent flow (the precise value depends on Re). Now the left-hand side of (10.48) is of order $C_0 C_\theta R^3$ while the right-hand side is at least of order $c_f C_\theta^2 R^3$. Thus (10.48) requires $C_0 \geq c_f C_\theta$, or equivalently $F_\theta \geq c_f |\mathbf{F}_p| \sim 0.01 |\mathbf{F}_p|$. This estimate was introduced earlier. It places a bound on the value of $F_\theta / |\mathbf{F}_p|$ below which an Ekman-dominated flow cannot be seen. If F_θ is less than this value, then the the induced swirl is too weak to counterbalance $\mathbf{F}_p$.

It appears, therefore, that an Ekman-dominated flow is physically realisable provided that F_θ is not too small. We shall see shortly that this is exactly what happens. When $F_\theta / |\mathbf{F}_p| < 10^{-3}$, $u_\theta \ll |\mathbf{u}_p|$. In the range $10^{-3} < F_\theta / |\mathbf{F}_p| < 10^{-2}$the swirl u_θ grows to be of order $|\mathbf{u}_p|$, and for $F_\theta / |\mathbf{F}_p| > 10^{-2}$the poloidal force is balanced by gradients in u_θ^2 / r and we get Ekman pumping, with $u_\theta \gg |\mathbf{u}_p|$. It is remarkable that the velocity field should be dominated by u_θ despite the relative weakness of F_θ.

Finally, we note that, in the arguments above, we have made no assumption about the direction of the poloidal force. We might anticipate, therefore, that the proposed solution works equally well for flows which (in the absence of F_θ) diverge at the surface, and we shall see that this is so in the next section. (Diverging surface flows may be created by a rather more elaborate arrangement of current injection.)

10.7.3 Some numerical experiments

We now describe a sequence of numerical experiments reported in Davidson et al. (1999). These relate to the flow of liquid steel in a hemispherical pool of radius $R = 0.1$ m. The flow was taken to be turbulent $(\mathrm{Re} \sim 10^5)$ and the Reynolds stresses τ_{ij} were estimated using the κ–ε turbulence closure model. The current distribution is controlled by the boundary condition set for $\mathbf{J}$, and the distribution used in the simulations is shown in Figure 10.9(a). The computations also allowed for an axial magnetic field $C_z = -C_0$, where C_0 lies in the range $0 \rightarrow 1$ m/s. The contours of constant F_r and F_θ (for $C_0 = 0.01$) are shown in Figure 10.9(b) and 10.9(c).

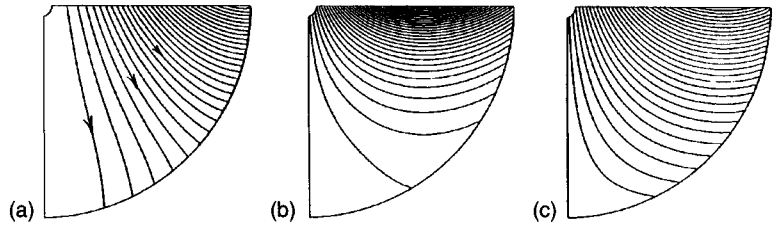

Figure 10.9 Current and forces in the liquid pool: (a) current; (b) contours of F_p, (c) contours of F_θ.

It is convenient to introduce the symbol $\hat{C}$ to represent the maximum value of C_θ. Note that $C_0/\hat{C}$ is a measure of the relative size of $F_\theta/|\mathbf{F}_p|$. With $\hat{C}$ fixed at 1 m/s, the flow was calculated for a range of values of $C_0/\hat{C}$, corresponding to 0, 0.005, 0.01, 0.02, 0.05, 0.1 and 1.0. This represents the full range from $F_\theta = 0$ to $F_\theta \sim |\mathbf{F}_p|$. The resulting variation of the kinetic energies E_θ and E_p (defined as the integrals of $u_\theta^2/2$ and $\mathbf{u}_p^2/2$) are shown in Figure 10.10. Note that, when the azimuthal force reaches a value of $\sim 0.01|\mathbf{F}_p|$, the swirl and poloidal motions have similar intensities. As F_θ is further increased, the energy of the poloidal motion collapses, dropping by a factor of 100. This is exactly the behaviour anticipated in Section 7.3.

The flow patterns for the cases $C_0 = 0$, 0.01 and 0.05 are shown in Figure 10.11. The transition to an Ekman-dominated structure is quite striking. For $F_\theta <\sim 0.01|\mathbf{F}_p|$, there is no Ekman pumping and the poloidal flow is dominated by $\mathbf{F}_p$, the swirl being too weak to react back on $\mathbf{u}_p$. For $F_\theta >\sim 0.01|\mathbf{F}_p|$ the poloidal flow is virtually eliminated through the balance $\mathbf{F}_p \sim -(u_\theta^2/r)\hat{\mathbf{e}}_r + \nabla\phi$. What little poloidal motion there is corresponds to Ekman pumping. Moreover, it is clear from Figure 10.10 that, for low values of F_θ, u_θ scales as $u_\theta \propto F_\theta$, which is what we would expect from (10.35). For large F_θ, on the other hand, we have $u_\theta \propto F_\theta^{5/9}$, which is typical of an Ekman flow (see Chapter 8).

The flows for the cases $C_0 = 0.1$ and 1.0 are shown in Figure 10.12 and compared with the case where the poloidal forcing is removed ($C_0 = 1.0$, $\hat{C} = 0$). Again, the motion is clearly dominated by Ekman pumping. It is remarkable that removing the poloidal forcing altogether makes almost no difference to the flow pattern. It is even more remarkable that, when the azimuthal forcing is only a few per cent of $\mathbf{F}_p$, the motion is dominated by swirl.

Finally, Davidson et al. (1999) considered a different distribution of $\mathbf{J}$, designed to drive a base flow, $\mathbf{u}_p$, which diverges at the surface. The

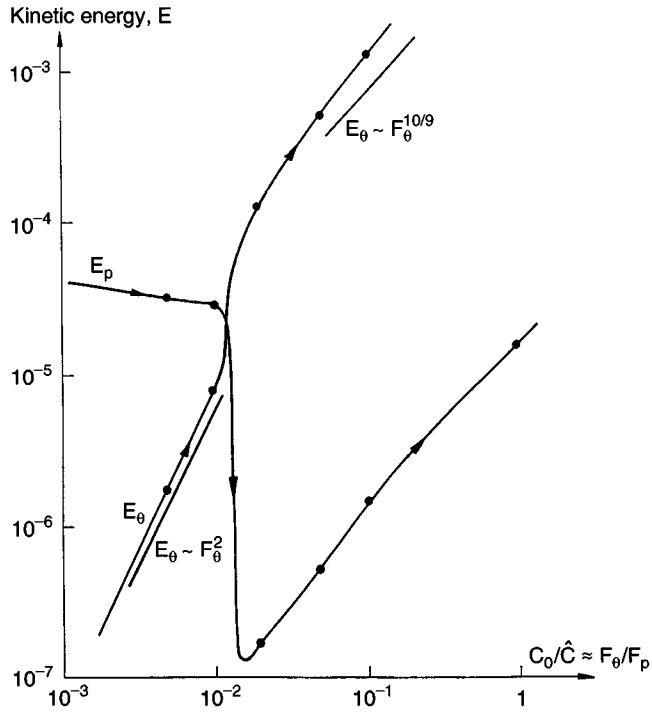

Figure 10.10 Variations of energy of the swirling (E_θ) and poloidal (E_p) components of motion as the ratio $F_\theta/|\mathbf{F}_p|$ is increased.

motivation here is to demonstrate that the phenomenon is quite unrelated to the direction of the poloidal base flow. Current was fed into the pool from the base and withdrawn at the sides. The resulting poloidal flow (in the absence of azimuthal forcing) then diverges at the surface. Nevertheless, they found precisely the same behaviour as before. When F_θ reaches a value of $\sim 0.01|\mathbf{F}_p|$ the energy of the poloidal motion collapses as an Ekman-dominated flow emerges.

These numerical experiments are broadly in line with the predictions of Section 7.1. It seems that the phenomenon of poloidal suppression is quite unrelated to the direction of the poloidal base flow and is not a manifestation of the breakdown of the self-similar solution. Rather, it results from a suppression of the poloidal motion through the balance $u_\theta^2/r \sim \mathbf{F}_p$. This allows the motion in the r–z plane to be dominated by Ekman pumping which, in turn, ensures that every streamline is flushed through the thin, dissipative Ekman layer. The result is a flow of low energy: E_p is virtually eliminated while $\mathbf{E}_\theta$ scales as $F_\theta^{10/9}$, rather than F_θ^2.

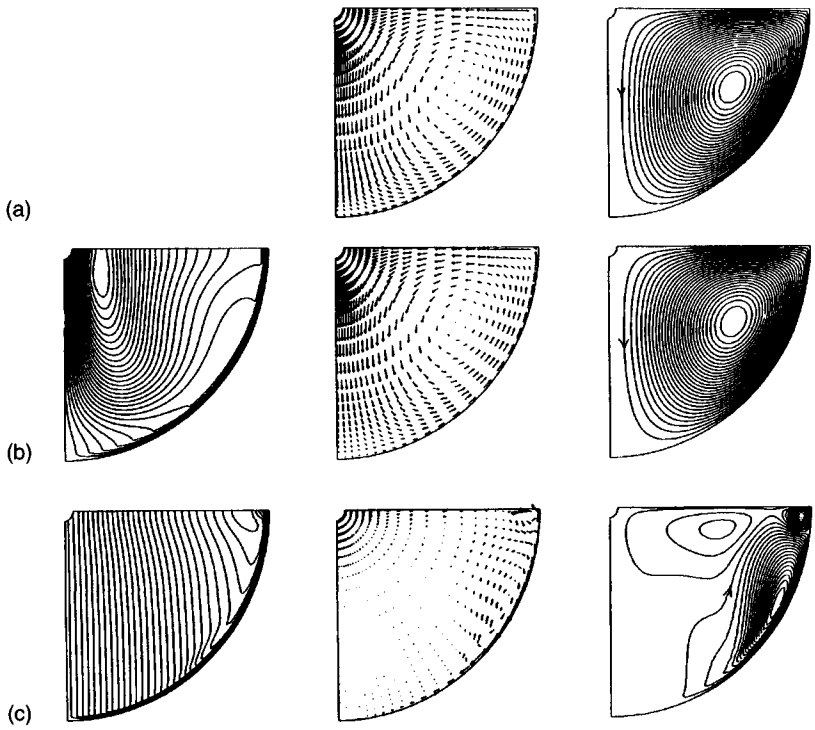

Figure 10.11 Contours of constant u_θ, poloidal velocity vectors and poloidal streamfunction for (a) $C_0 = 0$, (b) $C_0 = 0.01$ and (c) $C_0 = 0.05$.

Examples

10.1 Show that, for 2D flows, the global energy equation (10.3) is equivalent to evaluating the line integral (10.2) for each streamline and then adding all such integrals. Hint: consider a streamtube characterised by a jump in the stream-function $\delta\psi$, and then show that $u\delta A = \delta\psi dl$ where δA is an element of area with streamwise length dl.

10.2 Show that, for a point source of current on the surface of a semi-infinite domain,

$$B_\theta = \frac{\mu I}{2\pi r}(1 - \sin\phi)$$

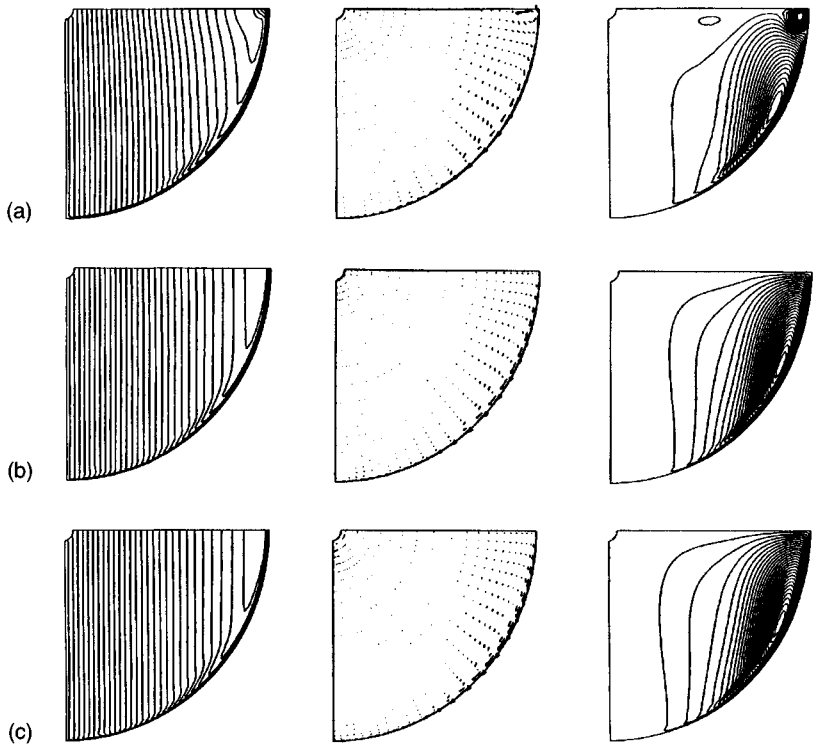

Figure 10.12 Contours of constant u_{θ}, poloidal velocity vectors and poloidal streamfunction for (a) $C_0 = 0.1$, $\hat{C} = 1.0$, (b) $C_0 = 1.0$, $\hat{C} = 1.0$ and (c) $C_0 = 1.0$, $\hat{C} = 0$.

10.3 The magnetic field used in the numerical experiments of Section 10.7.3 is

$$C_\theta = \hat{C} J_1(\delta_1 r/R) \cosh(\delta_1(1 - z/R))/[J_1(\delta_1)\cosh(\delta_1)]$$

Show that this corresponds to a current which leaves the cylinder $r < R$, $z < R$ normal to the surfaces $r = R$, $z = R$.